J Therm Anal Calorim (2012) 110:625–632
DOI 10.1007/s10973-011-1832-y

Study on thermal transformation of $CuHPO_4 \cdot H_2O$ obtained by acetone-mediated synthesis at ambient temperature

Rattanai Baitahe · Naratip Vittayakorn · Banjong Boonchom

Received: 10 July 2011 / Accepted: 28 July 2011 / Published online: 13 August 2011

Abstract Copper hydrogenphosphate monohydrate, $CuHPO_4 \cdot H_2O$, was synthesized for the first time through simple and rapid method using the mixing of copper carbonate and phosphoric acid in acetone medium at ambient temperature. The obtained $CuHPO_4 \cdot H_2O$ decomposed in three stages via dehydration and deprotonated hydrogenphosphate reactions, revealed by TG/DTG and DSC techniques. The kinetic triplet parameters (E_a, A, and n) and thermodynamic functions (ΔH^*, ΔG^*, and ΔS^*) for the first two decomposed steps were calculated from DSC data. All the obtained functions indicate that the deprotonated HPO_4^{2-} reaction for the second step occurs at a higher energy pathway than the dehydration reaction for the first step. The calculated wavenumbers based on DSC peaks were comparable with FTIR results, which support the breaking bonds of OH (H_2O) and P-OH (HPO_4^{2-}) according to decomposed mechanisms. All the calculated results are consistent and in good agreement with $CuHPO_4 \cdot H_2O$'s thermal transformation mechanisms.

Keywords Inorganic compounds · Chemical synthesis · Differential scanning calorimetry (DSC) · Thermodynamic properties

R. Baitahe · N. Vittayakorn
Electroceramic Research Laboratory, College of Nanotechnology, King Mongkut's Institute of Technology Ladkrabang, Bangkok 10520, Thailand

R. Baitahe · N. Vittayakorn
ThEP Center, CHE, 328 Si Ayutthaya Rd, Bangkok 10400, Thailand

N. Vittayakorn
Advanced Materials Science Research Unit, Department of Chemistry, Faculty of Science, King Mongkut's Institute of Technology Ladkrabang, Bangkok 10520, Thailand

B. Boonchom (✉)
King Mongkut's Institute of Technology Ladkrabang, Chumphon Campus, 17/1 M. 6 Pha Thiew District, Chumphon 86160, Thailand
e-mail: kbbanjon@gmail.com

Introduction

Copper phosphate compounds have been widely used in the area of catalysis, ion exchange, proton conductivity, food additive, fertilizer, detergent, fuel cell, intercalation chemistry, photochemistry, pigment, surface coating, and chemical materials [1, 2]. For interesting compounds, such as $CuHPO_4 \cdot H_2O$, $Cu_3(PO_4)_2 \cdot H_2O$, $Cu_2P_2O_7 \cdot 3H_2O$, $Cu_2P_2O_7$, $Cu_2P_4O_{12}$, and $Cu_3(PO_4)_2$ have been widely investigated due to their proper crystal structures and utilizations [3–6]. Most of their properties are dependent on the crystal type, crystalline, amorphous, morphology, shape, purity, and size. Consequently, a wide variety of copper phosphates have been synthesized to get appropriate properties. [5–20]. For example, $CuHPO_4 \cdot H_2O$ was synthesized from phosphoric acid and dicopper (II) dihydroxide carbonate at 333 K for 5 h [20], while $Cu_2P_2O_7$ was prepared from suitable copper salts and alkaline metal pyrophosphate salts ($A_2P_2O_7$; A = Na or K) by hydrothermal or high temperature (>573 K) [9–12]. $Cu_3(PO_4)_2 \cdot H_2O$ was prepared by a mixture of copper carbonate (56.42 wt% Cu) and H_3PO_4 solution (28.2 wt%) in a Teflon at 443 K for 24 h [12]. Whereas $Cu_2P_4O_{12}$ and $Cu_3(PO_4)_2$ were synthesized by heating the mixture systems of $CuCO_3 + Cu(OH_2) \cdot H_2O + 4H_3PO_4$ at 693 K for 1 h and $3CuCO_3 + Cu(OH_2) \cdot H_2O + 4H_3PO_4$ at 973 K for 1 h, respectively [3, 7].

Our interest in copper phosphate, $CuHPO_4{\cdot}H_2O$, has led us to search of new synthesis routes on organic solvent media. Organic molecules, methanol, ethanol, or acetone are widely used in the chemical synthesis, play an important role in shaping inorganic microcrystals and can influence the solubility and the crystallization kinetics (crystal nucleation and growth rate) of crystalline materials in solutions [2, 15–17]. Additionally, this copper phosphate is transformed to copper pyrophosphate, $Cu_2P_2O_7$, by dehydration and deprotonated hydrogen phosphate reactions (condensation) at high temperature. Therefore, the thermal stability of a chemical intermediate in connection with the thermal processing of this compound is one of the major fields of interest. So far, only mechanism of dehydration and condensation of the compound has been reported by Brandova et al. [20]. After a detailed literature survey, kinetic and thermodynamic studies of thermal transformation of the compound have been not found anywhere. The calculation of thermodynamic parameters from kinetic parameters is challenging and provides interesting new information, as exhibited in this article. These data play an important role in theoretical study for application development and industrial production of a compound as a basis of theoretical analysis.

The ambition of this work was to synthesize $CuHPO_4{\cdot}H_2O$ by acetone-mediated route at ambient temperature, which is a simple and cost-effective route. Thermal transformation of $CuHPO_4{\cdot}H_2O$ was observed by thermogravimetric analysis (TG/DTG) and differential scanning calorimetry (DSC), and the obtained results were analyzed from the kinetic and thermodynamic points of views. The relationship between kinetic parameters (E_a, n, and A) and thermodynamic functions (ΔH^*, ΔG^*, and ΔS^*) via the Kissinger method is reported on the basis of thermal analysis techniques. To the best of our knowledge, such a facile and acetone-mediated synthesis route, kinetic and thermodynamic studies as well as its physical meaning of thermal transformation of copper phosphate have not been reported.

Experimental

Synthesis and characterization

Copper hydrogen phosphate monohydrate, $CuHPO_4{\cdot}H_2O$ compound was prepared by acetone-mediated method using $CuCO_3$ (>99% purity, Merck), phosphoric acid (86.4%w/w H_3PO_4, Merck), and acetone (99.8%, Carlo Erba) as starting materials. In a successful synthesis run to yield $CuHPO_4{\cdot}H_2O$, 10 ml of acetone was first placed in a beaker containing 6.0 g of $CuCO_3$ and the formed opaque suspension was magnetically stirred at room temperature for 3 min, this suspension was referred to as mixture A. Then, 4 mL of 70% H_3PO_4 (81.02 mL of 86.4%w/w H_3PO_4 was dissolved in 18.98 mL of DI water) was added into the mixture A and then was vigorously stirred until the precipitates were completely obtained (15 min). The obtained pale blue powders were filtered by suction pump, washed with deionized water, dried at room temperature, and then kept in a desiccator.

Thermal analysis measurements (Thermogravimetry, TG; derivative Thermogravimetry, DTG) were conducted using a Perkin-Elmer, TGA Pyris 1 and Differential Scanning Calorimetry, DSC using a Perkin-Elmer DSC 204 F1 Phoenix apparatus with α-Al_2O_3 powder as the reference material. The structure and crystallite sizes of the prepared sample and its decomposed product were studied by X-ray powder diffraction using a D8 Advanced powder diffractometer (Bruker AXS, Karlsruhe, Germany) with Cu K_α radiation ($\lambda = 0.1546$ nm). The Scherrer method was used to evaluate the crystalline size [21]. The room temperature FTIR spectra were recorded in the range of 4,000–400 cm^{-1} with eight scans on a Perkin-Elmer Spectrum GX spectrometer with the resolution of 4 cm^{-1}. The morphology was examined by SEM using Hitachi S4700 after gold coating.

Kinetics and thermodynamics

Kinetic parameters of the dehydration and deprotonated hydrogenphosphate reactions of the synthesized $CuHPO_4{\cdot}H_2O$; namely the activation energy (E_a/kJ mol^{-1}) and frequency factor (A/s^{-1}) were calculated from differential scanning calorimetry (DSC) observed at different heating rates (5, 10, 15, and 20 K min^{-1}), using Kissinger's equation [22–24, 35–38]:

$$\ln\left(\frac{\beta}{T^2}\right) = -\frac{E_a}{RT} + \ln\left(\frac{E_a}{RA}\right) \quad (1)$$

where β is the heating rate (K min^{-1}), T is the DSC peak temperature, R is the gas constant (8.314 J mol^{-1} K^{-1}), A is the pre-exponential factor of Arrhenius (min^{-1}), and E is the activation energy (kJ mol^{-1}). Because of its easy use, the Kissinger method has been applied for determining the A and E parameters, which can be estimated by the slopes of the plots (E/R) and Y-intercepts, respectively [25]. The E and A values derived from the application of Eq. 1 imply a specific peak width and asymmetry if the reaction is first order. Correlations involving profile width and asymmetry relative to those of a first-order model can be used to estimate reaction order, nucleation order, or Gaussian distributed reactivity [26] models. These parameters are particularly useful to choose an appropriate model and initial guesses for mechanism by Eq. 2.

The thermal dehydration and deprotonated hydrogenposphate mechanisms could be determined from the shape

factor (n) of the endothermic DSC peak represented by the equation [23–28].

$$n = \frac{2.5}{\Delta D} \cdot \frac{T^2}{E_a/R} \tag{2}$$

where n is the Avrami constant, T is the endothermic DSC peak temperature, and ΔD is the full width at half maximum of the exothermic peak at four different heating rates.

Thermodynamic parameters, such as enthalpy change (ΔH/J mol^{-1}), heat capacity (C_p/J mol^{-1} K^{-1}), and entropy change (ΔS/J mol^{-1}K^{-1}), were calculated from DSC experiments carried out in N_2 atmosphere at the different heating rates. Thermodynamic functions were calculated by the following equations [29–31]:

$$\Delta S* = 2.303 C_p \log \frac{T_2}{T_1} \tag{3}$$

$$C_p = \frac{\Delta H*}{\Delta T} \tag{4}$$

$$\Delta H* = \frac{A}{\beta} \cdot \text{conts.} \tag{5}$$

$$\Delta G* = \Delta H* - T_p \Delta S* \tag{6}$$

when $\Delta T = T_2 - T_1$, T_1 is the temperature at which the DSC peak begins to depart the base line, and T_2 is the temperature at which the peak lands, T_p is the average phase transformation temperature peak in four DSC curves, A is peak area, and β is the constant heating rate.

The specificity of the thermal decomposition was characterized by identification of the bonds to be selectively activated due to energy absorption at vibrational level [32–34]. These breaking bonds were assigned and compared with the observed wavenumbers in the IR spectra. The relation between the kinetic parameter T_p and the wavenumbers of the activated bond is given as follows:

$$\omega = \frac{k_b}{hc} T_P = 0.695 T_p \tag{7}$$

where k_b and h are, respectively, the Boltzmann and Planck constants, and c the light velocity. Since the breaking bond has an unharmonic behavior, the specific activation is possible also due to more than one quanta, or by a higher harmonic: $\omega_{sp} = q\omega_{calc}$, $q \in N$, where ω_{sp} is the assigned spectroscopic number for the bond supposed to break.

Results and discussion

Characterization results

The TG/DTG curves of $CuHPO_4{\cdot}H_2O$ in air atmosphere are shown in Fig. 1. The TG curve shows the mass losses in the range of 303 and 923 K, which are related to water

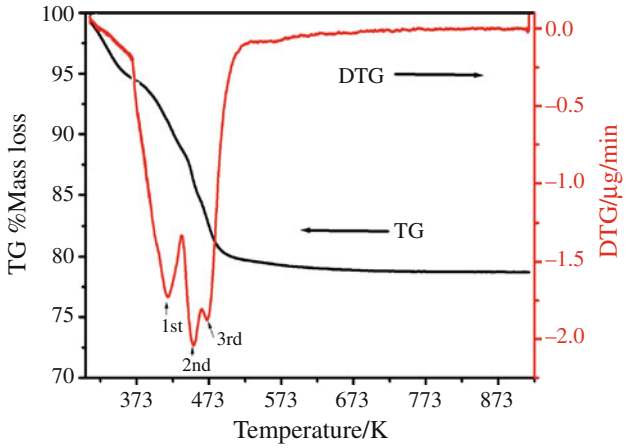

Fig. 1 TG/DTG curves of $CuHPO_4{\cdot}H_2O$ in N_2 at a rate of 10 K min^{-1}

molecules and changing of phase transformation. For losing water crystallization, dehydration steps observed in temperature areas of 373–434 K, 435–463 K, and 463–529 K correspond to mass losses of 6.03% (0.59 mol H_2O), 4.43% (0.44 mol H_2O), and 4.45% (0.44 molH_2O), respectively. These three stages shown on TG curve appear in the respective DTG and DSC as three peaks (415, 451, and 470 K). The total mass loss is 14.91% (1.47 molH_2O), which is very close to the theoretical value (15.21%; 1.50 mol H_2O). This confirms that the phosphate hydrate formula is $CuHPO_4{\cdot}H_2O$. The thermal decomposition of the synthesized $CuHPO_4{\cdot}H_2O$ involves dehydration of the coordinated water molecule (1 mol H_2O) and an intramolecular dehydration of the deprotonated hydrogenphosphate groups (0.5 mol H_2O), these processes formally could be presented as:

$$CuHPO_4{\cdot}H_2O \rightarrow CuHPO_4{\cdot}0.41H_2O + \sim 0.59H_2O \tag{8}$$

$$CuHPO_4{\cdot}0.41H_2O \rightarrow 1/2Cu_2P_2O_7{\cdot}H_2O + \sim 0.41H_2O \tag{9}$$

$$1/2Cu_2P_2O_7{\cdot}H_2O \rightarrow 1/2Cu_2P_2O_7 + \sim 0.50H_2O \tag{10}$$

Unstable intermediate compounds, acid hydrogen phosphates ($CuHPO_4{\cdot}0.5H_2O$ and $Cu_2P_2O_7{\cdot}H_2O$) have been registered. To gain the complete decomposition of synthesized $CuHPO_4{\cdot}H_2O$ in air atmosphere, the sample of $CuHPO_4{\cdot}H_2O$ was heated in a furnace at 573 K for 2 h and thermal transformation product was found to be $Cu_2P_2O_7$. These results confirmed by XRD and FTIR data are shown in Figs. 2 and 3. The absorbed water, thermal stability, mechanism, and phase transition temperature of $CuHPO_4{\cdot}H_2O$ obtained by acetone-mediated synthesis in this work are significantly different from those of $CuHPO_4{\cdot}H_2O$ reported in previous work [20]. The result clearly indicates that the thermal behaviors of materials

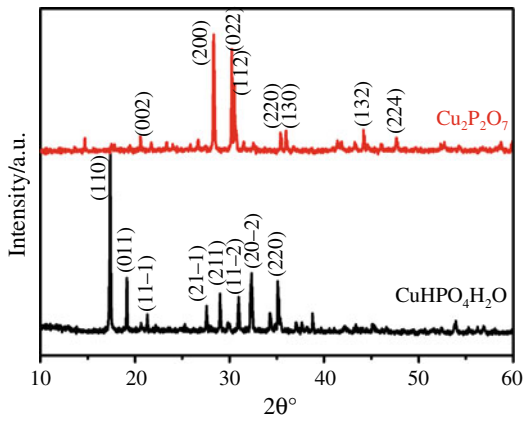

Fig. 2 XRD patterns of $CuHPO_4{\cdot}H_2O$ and its decomposition product $Cu_2P_2O_7$

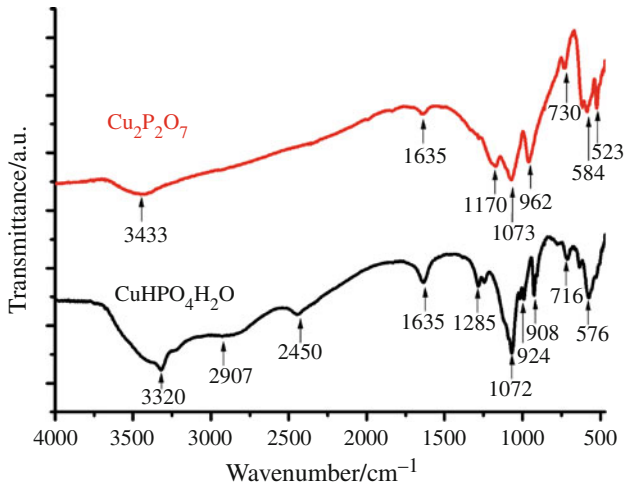

Fig. 3 FTIR spectra of $CuHPO_4{\cdot}H_2O$ and its decomposition product $Cu_2P_2O_7$

could be depended on synthetic method as well as condition reaction; reagents, media, pH, temperature and time.

The XRD patterns of $CuHPO_4{\cdot}H_2O$ and its decomposition product $Cu_2P_2O_7$ are shown in Fig. 2. All detectable peaks are indexed as the $CuHPO_4{\cdot}H_2O$ and $Cu_2P_2O_7$ with structure comparable to the standard data as PDF no. 83-1857 ($CuHPO_4{\cdot}H_2O$) and PDF no.21-0880 ($Cu_2P_2O_7$), respectively. The result indicated that both crystal structures are in monoclinic systems with space group $P2_1/a$ for $CuHPO_4{\cdot}H_2O$ and C2/c for $Cu_2P_2O_7$. The average crystallite sizes and lattice parameters of $CuHPO_4{\cdot}H_2O$ and $Cu_2P_2O_7$ were calculated from X-ray spectra broadening of the reflections using Scherrer equation (i.e. $D = 0.89\lambda/\beta\cos\theta$), where λ is the wavelength of X-ray radiation, θ is the diffraction angle, and β is the full width at half maximum (FWHM) [21] and tabulated in Table 1. The lattice parameters of $CuHPO_4{\cdot}H_2O$ and $Cu_2P_2O_7$ are comparable to those reported in the standard data.

The FT-IR spectra of $CuHPO_4{\cdot}H_2O$ and its decomposed product $Cu_2P_2O_7$ are shown in Fig. 3. The spectrum of $CuHPO_4{\cdot}H_2O$ illustrates the same characteristics as that of the fundamental vibrating units, HPO_4^{2-} and H_2O. The free H_2O molecule possesses C_{2v} symmetry. There are three normal modes of vibration: the symmetric ν_1 (A_1), the bending ν_2 (A_1), and the asymmetric ν_3 (B_2) vibrations. The symmetric ν_1 (A_1) and asymmetric ν_3 (B_2) of HOH in title compound was observed at 3,320 and 3,100 cm^{-1}, respectively. The bending vibration of water molecules appears at 1,635 cm^{-1} and a weak band at approximately 630 cm^{-1} is assigned to water libration (rocking mode). Vibrational bands of HPO_4^{2-} ion are observed in the regions of 300–3,000 cm^{-1}. Typical vibrations of title compound is the appearance of the characteristic ABC structure of the ν (OH) vibration bands [3, 5, 7, 10, 11] because of the existence of a variety of strongly hydrogen-bonded solid. The problem of the origin of the *ABC* trio is discussed in many studies on acidic salts, but an explanation of this behavior of strongly hydrogen-bonded systems is still to be found [3, 5]. One of the most popular interpretations of the *ABC* trio suggests a strong Fermi resonance between the ν(OH) stretching fundamentals and the overtones [2δ(OH) and 2γ(OH)] or combinations involving the δ(OH) and γ(OH) vibrations. Usually, the *ABC* bands

Table 1 Average crystallite sizes and lattice parameters of $CuHPO_4{\cdot}H_2O$ and $Cu_2P_2O_7$ calculated from XRD data

Compounds	Systems	*a*/nm	*b*/nm	*c*/nm	β/°	Average crystallite size/nm
$CuHPO_4{\cdot}H_2O$	PDF no. 83-1857	0.8606	0.6346	0.6811	94.160	–
	This work	0.8625 (3)	0.6345 (2)	0.6810 (4)	94.236 (0)	93 ± 25
Dif: This work − PDF		−0.0019	0.0001	0.0001	−0.0076	
$Cu_2P_2O_7$	PDF no.21-0880	0.6876	0.8113	0.9162	109.540	–
	This work	0.6861(0)	0.8207(0)	0.9209(1)	109.79(3)	97 ± 19
DIF: This work − PDF		0.0015	−0.0094	−0.0047	−0.250	

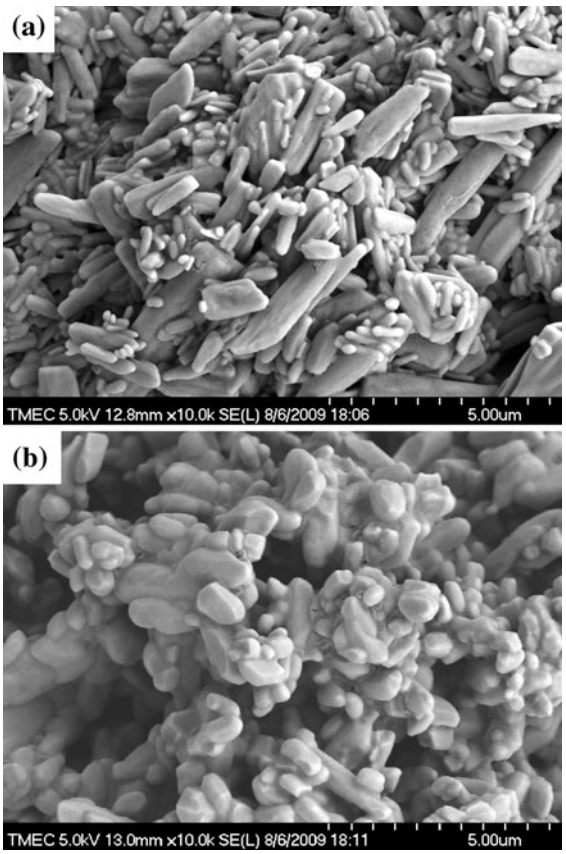

Fig. 4 SEM micrograph of $CuHPO_4 \cdot H_2O$ (**a**) and its decomposition product $Cu_2P_2O_7$ (**b**)

are very broad and consist of many ill-resolved components. Two bands centered at 2,907 and 2,450 cm^{-1} in the FTIR spectrum are referred to as bands A and B, respectively. The third component (band C) is observed around 1,749–1,639 cm^{-1}. The typical intense bands at about 1,285 cm^{-1} is due to the in plane P–O–H bending (A_2), while the out of plane bending (A_1) vibration is observed at about 908 cm^{-1}. Consequently, the acidity of $CuHPO_4 \cdot H_2O$ has the reason of high catalytic activity to remain a point of contentions. Vibrational spectra of present hydrate were assigned by factor group analysis and derived from the same mode in the free HPO_4^{2-} ion. A strong band at about 1,072 cm^{-1} in FTIR spectra is assigned to PO_3 symmetric stretching (B_1). The FTIR frequency of the PO_3 symmetric stretching (A_1) shows the strong band at about 924 cm^{-1}. The weak and broader band at about 576 cm^{-1} is corresponding to PO_4 (E) and P-OH (A_1) bending modes.

The FTIR spectrum of the $CuHPO_4 \cdot H_2O$ calcined at 573 K (Fig. 3) has been reported that the degree multiplication and fineness in the spectra of phosphates increase as the degree of polymerization increases in the tetrahedral $[PO_3]^{3-}$ [3, 5, 7, 10, 11]. It is clearly noticed that the studied compounds exhibit more splitting and sharpness, especially in the low-frequency region, indicating polymerization of $[PO_4^{3-}]$ to $[P_2O_7]^{4-}$. The strong vibration bands at 1,170 and 1,073 cm^{-1} are attributed to the stretching of PO_3 unit. The asymmetric (ν_{asym} POP) and symmetric stretch (ν_{sym} POP) bridge vibration for this sample are observed at about 962 and 730 cm^{-1}, while the asymmetric (δ_{asym} PO_3) and symmetric (δ_{sym} PO_3) bending vibration are observed at about 584 and 523 cm^{-1}, respectively. The PO_3 determination, rocking mode of the POP deformations, the torsional and external modes are found in the 400–230 cm^{-1} region.

The changing morphologies of $CuHPO_4 \cdot H_2O$ and its decomposition product $Cu_2P_2O_7$ are shown in Fig. 4. The SEM micrograph of $CuHPO_4 \cdot H_2O$ (Fig. 4a) illustrates many small and some large rod-like microparticles, which were about 0.4–2.0 μm in length and 0.1–0.5 μm in width and about 1.5–7.0 μm in length and 0.5–1.0 μm in width, respectively. The SEM micrograph of $Cu_2P_2O_7$ (Fig. 4b) shows retexturing and coalescence in aggregates of non-polyhedral shaped crystals of different sizes in the range of 1.0–5.0 μm.

Kinetics and thermodynamic studies

Figure 5 shows the DSC curves of $CuHPO_4 \cdot H_2O$ at four heating rates that the data were collected to calculate the values of kinetics and thermodynamic parameters according to the Eqs. 1–6. A summary of the parameters obtained in this calculation, including kinetic triplet parameters (E_a, A, n) and thermodynamic functions (C_p, ΔH^*, ΔS^*, ΔG^*) for only the first and the second steps, is given in Table 2. The activation energies of dehydration (step I) and

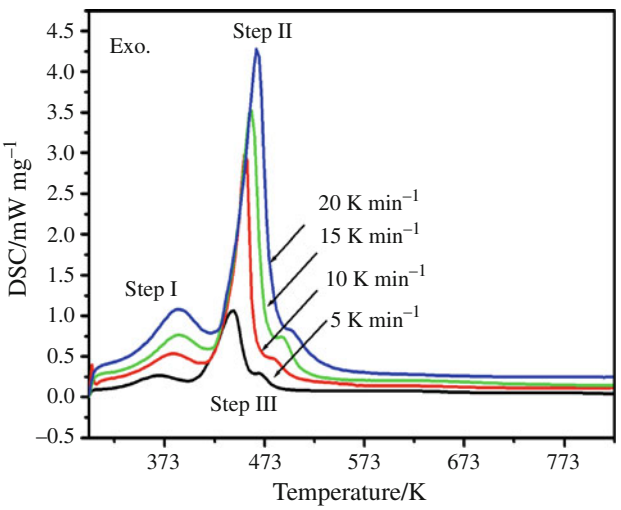

Fig. 5 DSC curves of $CuHPO_4 \cdot H_2O$ in a N_2 atmosphere at the four heating rates (5, 10, 15, and 20 K min^{-1})

Table 2 Kinetics and thermodynamics of $CuHPO_4{\cdot}H_2O$ in a N_2 atmosphere

Step	C_p/kJ mol^{-1}K^{-1}	ΔG^*/kJ mol^{-1}	ΔH^*/kJ mol^{-1}	ΔS^*/J mol^{-1}K^{-1}	A/s^{-1}	E_a/kJmol^{-1}	n	R^2	T_{ap}/K	ω_{cal}	q	$q\omega_{cal}$/cm^{-1}	Band assignment
1	0.08	−1.92	6.97	0.08	6.98×10^5	65.60	1.24	0.9965	415	288	6	1730	ν_2 (H_2O) or C band ($H_2PO_4^-$)
											11	3172	ν_1 (H_2O)
											12	3461	ν_3 (H_2O)
2	0.43	5.31	59.37	0.30	8.55×10^7	97.04	2.28	0.9983	451	200	4	802	ν (P-OH)
											6	1202	$\nu_s(PO_2)$
											12	1603	ν_2 (H_2O) or C band ($H_2PO_4^-$)
											15	2405	B band ($H_2PO_4^-$)
											16	3006	A band ($H_2PO_4^-$)
											17	3207	ν_3 (H_2O)

deprotonated hydrogenphosphate (step II) reactions were found to be 65.60 kJ mol^{-1} ($r^2 = 0.9965$) and 97.04 kJ mol^{-1} ($r^2 = 0.9983$), respectively. The activation energy value for deprotonated hydrogenphosphate reaction is higher than that of dehydration reaction, which indicated that the second step is harder than the first step. The similar results of the pre-exponential factor, which is used to measure the collision frequencies, reveal that the second step shows much higher collision frequencies compared with the first step. Therefore, deprotonated hydrogenphosphate reaction should occur at an even higher-energy pathway. The n values of the two decomposition steps were found to be 1.24 and 2.28, respectively. Furthermore, this also implies that the second step should be interpreted to occur by a more complicated mechanism than that of the first step. Values of $n \approx 3$, 2, and 1 indicate 3D growth (spheres or hemispheres), 2D growth (disks and cylinders), and linear growth [23–28], respectively. Based on these results, the observed n values in this study suggest that the dehydration and deprotonated hydrogenphosphate reactions are dominated by a surface decomposition mechanism rather than by volume decomposition and that the decomposition dimension is low [30] (1D growth and 2D growth, respectively), which indicates that it is a nucleation-controlled mechanism.

For thermodynamics functions, the formation of the activated complex of the reagent reflects in a specific way the change of the entropy (ΔS^*). As can be seen from Table 2, the entropy of activation (ΔS^*) values for the first ($\Delta S^* = 0.08$ kJ mol^{-1}) and second ($\Delta S^* = 0.30$ kJ mol^{-1}) steps are positive. A positive entropy values indicate that the transition states are highly disordered compared with the initial state ($CuHPO_4{\cdot}H_2O$). It means that the corresponding activated complexes have a lower degree of arrangement than the initial state. Since the decomposition of $CuHPO_4{\cdot}H_2O$ proceeds as two consecutive reactions, the formation of the second activated complex passed in situ. In terms of the theory of activated complexes (transition theory) [28–31, 34–38], a positive value of ΔS^* indicates a malleable activated complex that leads to a large number of degrees of freedom of rotation and vibration. The result may be interpreted as a "fast" stage. On the other hand, a negative value of ΔS^* indicates a highly ordered activated complex, and the degrees of freedom of rotation as well as of vibration are less than they are in the non-activated complex. This result may indicate a "slow" stage [28–31, 34–38]. Therefore, the dehydration (1st) and deprotonated hydrogenphosphate reactions (2nd) of the thermal decomposition of $CuHPO_4{\cdot}H_2O$ may be interpreted as "fast" stages. For the enthalpy ΔH^*, positive values are in good agreement with two endothermic effects in the DSC data. The relationship of activation energy, E_a, and change of enthalpy, ΔH^*, of the two decomposition steps show that the ΔH^* value of the second deprotonated hydrogenphosphate step

($\Delta H^* = 59.37$ kJ mol^{-1}) is higher than that of the first dehydration step ($\Delta H^* = 6.97$ kJ mol^{-1}), which also results in the same effect in the ΔH^* value and indicated that the second step needs a higher-energy pathway than the first step. The negative and positive values of ΔG^* for the dehydration ($\Delta G^* = -1.92$ kJ mol^{-1}) and second deprotonated hydrogenphosphate ($\Delta G^* = 5.31$ kJ mol^{-1}) stages indicate spontaneous and non-spontaneous processes, respectively. The ΔG^* values indicate that the second step needs a higher-energy pathway than the first step. On the basis of thermodynamic results, we can conclude that the second decomposition step is harder reaction, more difficulty and lower rate than the first decomposition step. The result is consistent with the deprotonated hydrogenphosphate reaction occurring at the breaking of the strong hydrogen-bonded P-OH group in this structure, which confirms that decomposition product as copper pyrophosphate ($Cu_2P_2O_7$).

To corroborate the calculated wavenumbers according Eq. 7 with the spectroscopic ones, we drew up the FTIR spectra of the studied compound (Fig. 3). Table 2 shows the comparison of the ω_{calc} values with the ω_{sp} values determined from two steps of this compound, together with the assignments of the vibrational modes related in the literature [32]. The results indicate that the breaking bonds of O–H for H_2O molecules occur in the first step, which is referred to the dehydration reactions. Whereas the breaking bonds of the true P-OH for the $H_2PO_4^{2-}$ units occur in the second step, which is referred to a continuous intermolecular polycondensation and then eliminated water molecules. The calculated wavenumbers from average T_p (DSC) are consistent with the observed wavenumbers from FTIR spectra, which suggest broken bond for the thermal transformation in each step. The calculated results are in good agreements with thermal mechanism, kinetic, and thermodynamic data.

Conclusions

Copper hydrogen phosphate monohydrate, $CuHPO_4 \cdot H_2O$ was obtained by a rapid and simple acetone-mediated synthesis using phosphoric acid and copper carbonate at ambient temperature with short time consuming (15 min). Thermal transformation of $CuHPO_4 \cdot H_2O$ occurs through the dehydration and deprotonated hydrogenphosphate reactions and its final product, copper pyrophosphate ($Cu_2P_2O_7$) was obtained at 573 K. The prepared $CuHPO_4 \cdot H_2O$ and $Cu_2P_2O_7$ products were confirmed by XRD, FTIR, and SEM techniques, which are important for their further treatments. The kinetics and thermodynamics of the thermal decomposition of $CuHPO_4 \cdot H_2O$ were studied using non-isothermal DSC applying model-fitting method, which have attracted the interest of kinetics and thermodynamic scientists. Results exhibit that kinetic triplet parameters (E_a, A, n) and thermodynamic functions (C_p, ΔH^*, ΔS^*, ΔG^*) indicate the loss of water of crystallization for the first step and elimination of water of constituent in hydrogenphosphate anion for the second step. This obtained research displays that the simple, rapid, and cost-effective method is necessary for elaboration of technology and academic scientist to produce the copper phosphates, which plays a large role in industrial applications.

Acknowledgements This work financially supported by the National Nanotechnology Center (NANOTEC) NSTDA, Ministry of Science and Technology, Thailand.

References

1. Averbuch-Pouchat MT, Durif A. Topics in phosphate chemistry. 1st ed. Singapore: World Scientific; 1996.
2. Xu J, Zhang J, Qian J. Hydrothermal synthesis of potassium copper phosphate hydrate and ludjibaite microcrystals. J Alloys Compd. 2010;494:319–22.
3. Onoda H, Okumoto K-I, Nakahira A, Tanaka I. Mechanochemical effects on the synthesis of copper orthophosphate and *cyclo*-tetraphosphate bulks by the hydrothermal hot pressing method. Materials. 2009;2:1–9.
4. Galkova TN, Pacewska B, Samuskevich VV, Pysiak J, Shulga NV. Thermal transformations of $CuNH_4PO_4 \cdot H_2O$. J Therm Anal Calorim. 2000;60:1019–32.
5. Frost RL, Kloprogge T, Williams PA, Martens W, Johnson TE, Leverett P. Vibrational spectroscopy of the basic copper phosphate minerals: pseudomalachite, ludjibaite and reichenbachite. Spectrochim Acta A. 2002;58:2861–8.
6. Lucheva B, Tsonev TS, Petkov R. Method for obtaining of copper-phosphorus alloys. J Univ Chem Technol Metall. 2005; 40:235–8.
7. Onoda H, Okumoto K-I, Tanaka I. Mechanochemical reforming of powder and acidic properties of copper *cyclo*-tetraphosphates. Mater Chem Phys. 2008;107:339–43.
8. Bamberger CE, Specht ED, Anovitz LM. Crystalline copper phosphates: synthesis and thermal stability. J Am Ceram Soc. 1997; 80(12):3133–8.
9. Robertson BE, Calvo C. The crystal structure and phase transformation of α-$Cu_2P_2O_7$. Acta Crystallogr. 1967;22:665–72.
10. Effenberger H. Structural refinement of low-temperature copper(II) pyrophosphate. Acta Crystallogr. 1990;C46:691–2.
11. Navrotsky SN, Le A, Pralong V. Energetics of copper diphosphates—$Cu_2P_2O_7$ and $Cu_3(P_2O_6OH)_2$. J Solid State Sci. 2008; 10:761–7.
12. Viter VN, Nagornyi PG. Synthesis and characterization of $(Cu_{1-x}Zn_x)_3(PO_4)_2 \cdot H_2O$ $(0 < x \leq 0.19)$ solid solutions. Inorg Mater. 2006;42(4):406–9.
13. Bamberger CE, Specht ED, Anovitz LM. Compounds and solid solutions of cobalt, copper phosphates. J Am Ceram Soc. 1998; 81(11):2799–804.
14. Kopilevich VA, Zhilyak ID, Voitenko LV. Synthesis and thermal transformations of hydrated ammonium copper(II) zinc diphosphate. Russ J Appl Chem. 2005;78(12):1917–20.
15. Prokopchuk NN, Kopilevich VA, Voitenko LV. Preparation of double nickel(II) cobalt(II) phosphates with controlled cationic composition. Russ J Appl Chem. 2008;81(3):386–91.

16. Bhatgadde LG, Mahapatra S. Preparation and optimization of pyrophosphate bath for copper electroplating of microwave components. Def Sci J. 1988;38(2):119–23.
17. da Silva Filho EC, da Silva OG, da Fonseca MG, Arakaki LNH, Airoldi C. Synthesis and thermal characterization of copper and calcium mixed phosphates. J Therm Anal Calorim. 2007;87(3): 775–8.
18. Podgornova L, Kuznetsov P, Yu I, Gavrilova SV. On the zinc and copper dissolution in phosphate solutions. Prot Met. 2003;39(3): 217–21.
19. Ciopec M, Muntean C, Negrea A, Lupa L, Negrea P, Barvinschi P. Synthesis and thermal behavior of double copper and potassium pyrophosphate. Thermochim Acta. 2009;488:10–6.
20. Brandová D, Trojan M, Arnold M, Paulik F, Paulik J. Mechanism of dehydration and condensation of $CuHPO_4 \cdot H_2O$. J Therm Anal Calorim. 1988;34:1449–54.
21. Cullity BD. Elements of X-ray diffraction. 2nd ed. Massachusetts: Addison-Wesley; 1977.
22. Kissinger HE. Reaction kinetics in differential thermal analysis. Anal Chem. 1957;29:1702–6.
23. Anilkumar GM, Sung YM. Phase formation kinetics of nanoparticle-seeded strontium bismuth tantalate powder. J Mater Sci. 2003;38:1391–6.
24. Zhao MS, Song XP. Synthesizing kinetics and characteristics for spinel $LiMn_2O_4$ with the precursor using as lithium-ion battery cathode material. J Power Sources. 2007;164:822–8.
25. Brown ME, Maciejewski M, Vyazovkin S, Nomen R, Sempere J, Burnham A, Opfermann J, Strey R, Anderson HL, Kemmler A, Keuleers R, Janssens J, Desseyn HO, Li C-R, Tang TB, Roduit B, Malek J, Mitsuhashi T. Computational aspects of kinetic analysis Part A: the ICTAC kinetics project-data, methods and results. Thermochim Acta. 2000;355:125–43.
26. Vyazovkin S, Burnham AK, Criado JM, Perez-Maqueda LA, Popescu C, Sbirrazzuoli N. ICTAC kinetics committee recommendations for performing kinetic computations on thermal analysis data. Thermochim Acta. 2011;520:1–19.
27. Zhang LM, Chen D, Wu J. Leucite crystallization kinetics with kalsilite as a transition phase. Mater Lett. 2007;61:2978–81.
28. Boonchom B. Kinetics and thermodynamic properties of the thermal decomposition of manganese dihydrogenphosphate dehydrate. J Chem Eng Data. 2008;53:1533–8.
29. Cordes HM. Preexponential factors for solid-state thermal decomposition. J Phys Chem. 1968;72:2185–9.
30. Young D. Decomposition of solids. Oxford: Pergamon Press; 1966.
31. Turmanova SCh, Genieva SD, Dimitrova AS, Vlaev LT. Non-isothermal degradation kinetics of filled with rise husk ash polypropene composites. Express Polym Lett. 2008;2:133–46.
32. Herzberg G. Molekülspektren und Molekülstruktur. I. Zweiatomige Moleküle. Dresden: Steinkopff; 1939.
33. Colthup NB, Daly LH, Wiberley SE. Introduction to infrared and Raman spectroscopy. New York: Academic Press; 1964.
34. Vlase T, Vlase G, Doca M, Doca N. Specificity of decomposition of solids in non-isothermal conditions. J Therm Anal Calorim. 2003;72:597–604.
35. Bertol C, Cruz A, Stulzer H, Murakami F, Silva M. Thermal decomposition kinetics and compatibility studies of primaquine under isothermal and non-isothermal conditions. J Therm Anal Calorim. 2010;102:187–92.
36. Navarro M, Lagarrigue M, De J, Carbonio R, Gómez M. A new method of synthesis of $BiFeO_3$ prepared by thermal decomposition of $Bi[Fe(CN)_6] \cdot 4H_2O$. J Therm Anal Calorim. 2010;102:655–60.
37. Boonchom B, Danvirutai C. Kinetics and thermodynamics of thermal decomposition of synthetic $AlPO_4 \cdot 2H_2O$. J Therm Anal Calorim. 2009;98:771–7.
38. Mansurova A, Gulyaeva R, Chumarev V, Mar'evich V. Thermochemical properties of $MnNb_2O_6$. J Therm Anal Calorim. 2010;101:45–7.